Study of an overmoded structure for megawatt *Ka*-band extended interaction klystron ⊘

Yifan Zu ; Xuesong Yuan ✉ ; Xiaotao Xu; Qingyun Chen; Matthew T. Cole ; Yong Yin ; Hailong Li ; Bin Wang; Lin Meng; Yang Yan

Check for updates

View Online   Export Citation   CrossMark

Study of an overmoded structure for megawatt *Ka*-band extended interaction klystron

View Online　　Export Citation　　CrossMark

Yifan Zu,[1] (ID) Xuesong Yuan,[1,a)] (ID) Xiaotao Xu,[1] Qingyun Chen,[1] Matthew T. Cole,[2] (ID) Yong Yin,[1] (ID) Hailong Li,[1] (ID)
Bin Wang,[1] Lin Meng,[1] and Yang Yan[1]

AFFILIATIONS

[1]Terahertz Science and Technology Key Laboratory of Sichuan Province, School of Electronic Science and Engineering,
University of Electronic Science and Technology of China, Chengdu 610054, China
[2]Department of Electronic and Electrical Engineering, University of Bath, North Road, Bath BA2 7AY, United Kingdom

[a)]Author to whom correspondence should be addressed: yuanxs@uestc.edu.cn

ABSTRACT

For most applications in the millimeter wave band, corresponding to *Ka* and higher-frequency bands, relatively high atmospheric absorption necessitates the use of high-power sources. Here, a new approach for projecting an oversized beam tunnel in an overmoded structure by concentrating the axial field is demonstrated to meet the high-frequency and high-power demands of compact devices. Due to the enhanced intense beam loading capability of the interaction circuit, a six-cavity *Ka*-band extended interaction klystron with a four-coupling-hole disk-loaded structure is designed that can stably obtain high output power. An analysis of optimization tradeoffs from introducing high order modes for allowing the application of more powerful beams to improving high order mode field distribution for enhancing the electron-wave coupling and suppressing mode competition is reported. 3D particle-in-cell simulations show attainable output powers of 1.11 MW at 32.94 GHz with a saturated gain of 57 dB by injecting a 3.3 mm diameter electron beam with a current of 24 A.

Published under an exclusive license by AIP Publishing. https://doi.org/10.1063/5.0163920

I. INTRODUCTION

Advances in microwave and millimeter wave technology are driving the continued development of advanced diagnostic technologies, including radio astronomy, biomedical research instruments, high resolution radar, and plasma diagnostics.[1–6] In some applications, there are clear advantages to the use of higher frequencies.[7] When designing next-generation acceleration drivers, higher drive frequencies generally allow for higher operating field gradients. This significantly reduces the volume and construction cost of the accelerator.[8,9] Millimeter wave band enables radar designers to achieve higher energy density and improved angular resolution in space with practical transmitter power and antenna aperture, while employing wide instantaneous bandwidth, and gain increased Doppler frequency shifts for a specified radial velocity spread.[10,11] High-power density and localization, which make millimeter-wave systems attractive, will also enable smaller fusion research devices to play an important role in the development of new energy resources.[12,13] Progress in these fields rests critically on the development of high-power electronics in the millimeter wave band.

The quest for higher peak power has spurred interest in the production of microwave power using relativistic electron beams.[5,14] However, the practical applicability of short-pulse high-power relativistic devices is often limited by their short lifetime and stability as a result of the restricted number of pulses that can be generated using explosive emission cathodes and the formation of unnecessary but damaging plasma on the high-frequency metallic structures and output windows.[14] Furthermore, device power density performance has a strong emphasis on average power production at higher frequencies. Extended interaction klystrons (EIKs) are one of the most competitive high-power devices in the family of vacuum electronic devices.[15–17] Due to their general construction from multiple multi-gap cavities, EIKs have high circuit impedance and considerable output power and interaction efficiency.[18] Therefore, at high frequencies, EIKs not only have higher gain-bandwidth product than the traditional klystrons but also have a shorter total circuit length than traveling wave tubes.[19] Moreover, the compactness of EIKs further reduces device weight and volume due to lower magnetic field requirements than gyrotrons. While the EIK holds great promise as a high-power source, there are still many challenges to be solved, which mainly share many of the same plasma physics challenges faced by high-power microwave generators.[20] With the expansion of devices into the millimeter wave regime and higher frequency bands, high-frequency structures will become extremely small due to the co-transition effect of

device structure size and operating wavelength. The compact size has a number of production challenges and, in principle, requires the electron beam to have tiny transverse dimensions and potentially very high current densities, likely in excess of 300 A/cm², to maintain sufficiently high gain and power.[21] Therefore, current challenges about the micro-fabrication of interaction circuits are perhaps surpassed by the difficulties in producing small diameter, high current, precisely aligned electron beams. Not only that, the strong electric fields concentrated in the small cavity will inevitably increase the risk of breakdown and arcing, which affects stable operation of the device.

In this paper, an overmoded high frequency interaction circuit is presented. The power limitation imposed by cross-sectional dimensions, which shrink with wavelength, can be overcome by using cavities and waveguides that are much larger than the wavelength in the transverse dimension due to operation in higher-order modes.[22–29] By realizing the method of concentrating the axial field energy along the source's central axis within a large cavity, an oversized beam tunnel that can supports efficient energy conversion between the intense electron beam and the high frequency field is designed. This overmoded structure has a far larger electron beam loading area than conventional structures.[30–32] In Sec. II, a basic interaction structure operating in the quasi-TM$_{02}$ mode and its field distribution are described. In Sec. III, a trade-off analysis from introducing high order modes for achieving the larger circuit size to improving high order modes field distribution for maintaining sufficient electron-wave coupling and suppress mode competition is reported. In Sec. IV, the stability and beam–wave interaction capability of the *Ka*-band EIK based on the overmoded structure are verified by 3D particle-in-cell (PIC) simulations. Conclusions are covered in Sec. V.

II. DESIGN OF THE OVERMODED CIRCUIT

For conventional linear beam devices, as the interaction circuits become smaller as the frequency extends into the millimeter wave band, a smaller electron beam is essential to keep the beam diameter smaller than the device operating wavelength. However, for a practical electron-optical system to be optimized for lifetime and electrical stresses, the current density emitted from the cathode must remain within a reasonable range, and the compression of the beam must be limited. Thus, the beam current is inevitably limited by the transverse size, which results in a significant reduction in output power. Here, enlarging the diameter of the beam tunnel to accommodate the high-

current intense electron beam has become the technical key to solve the power limitation of millimeter-wave linear beam devices.

With the increasing demand for high power in compact high frequency devices, insights gained using overmoded structures in fast-wave device development can be extended to linear beam devices typified by EIKs.[22] Compared with the commonly used fundamental mode, the most significant feature of the higher-order mode is that it can support a physically larger interaction system for a given frequency.[33] From the Bessel function field of circular waveguide and cylindrical cavity resonator, the higher the TM mode order, the more concentrated the E_z-field strength in the axial central region.[34] The concentration of the axial electric field not only improves the beam–wave interaction but also makes it possible to expand the diameter of the beam tunnel. After preliminary empirical analysis, the TM$_{02}$-based mode is selected. Figures 1(a) and 1(b) show the E_z-field distribution at the cross section of a single interaction gap. The established operating mode exhibits the strongest E_z-field distribution at and near the central axis, which enhances the interaction with the electron beam passing through the central axis.

Combining the field distribution established by the axisymmetric circular waveguide and the cylindrical cavity resonator, a novel disk-loaded structure with four coupled holes is proposed, as shown in Fig. 2(a). The core technology of this structure is the introduction of periodically superimposed center disks. Since the central disk cannot be suspended in the cavity, fan-shaped coupling holes are formed between the supporting plates connected with the inner wall of the cavity. The four fan-shaped coupling holes are evenly distributed in an axisymmetric manner. Adjacent interaction gaps are coupled and communicated through coupling holes. In addition, coupling holes have the effect of adjusting the distribution of the mode field. It is worth noting that the numerous geometric parameters of the disk-loaded structure with coupling holes provide a corresponding degree of flexibility for defining various technical figures of merit of the circuit and for the subsequent high frequency characteristics assessment.

Table I lists the initial design parameters of the two structures shown in Fig. 2, respectively. The differences between the two structures are discussed in detail in Sec. III due to the issue of mode competition related to beam–wave interactions. Here, the two structures belong to the category of four-coupling-hole disk-loaded structures, and both have four fan-shaped coupling holes distributed symmetrically about the axis and an electron beam tunnel opened at the center.
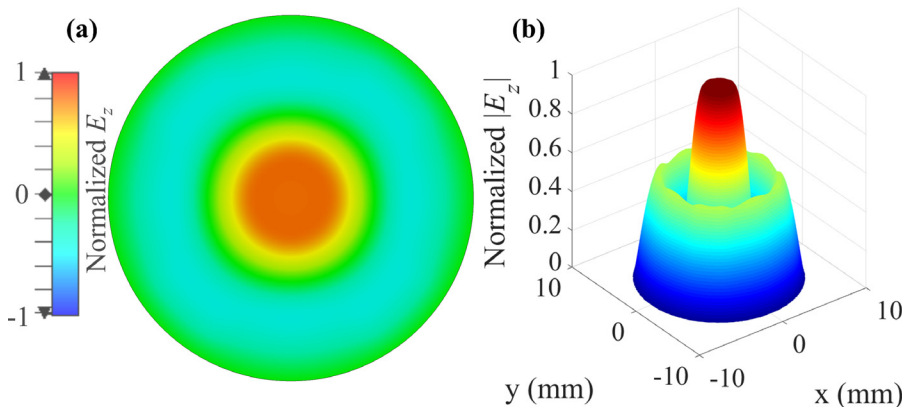
(a)

(b)

FIG. 1. (a) E_z-field distribution and (b) $|E_z|$-field contour plot of the quasi-TM$_{02}$ mode at z = 0 plane.
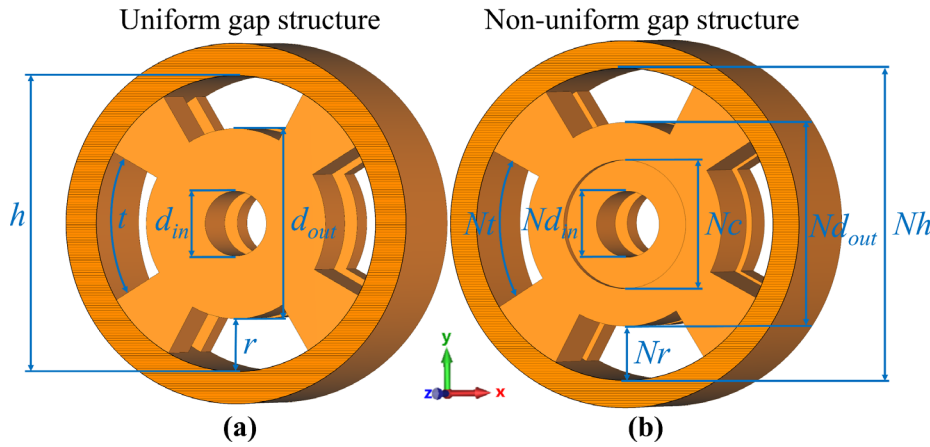
FIG. 2. Model dimensions for (a) uniform gap structure (UGS) and (b) non-uniform gap structure (NUGS).

Since the two structures have the same resonant frequency, as shown in Table I, if the coupling hole radius and the electron beam tunnel diameter of the two structures are kept the same, the remaining parameters of the structures will show slight differences. Note that the beam tunnel diameter of the designed four-coupling-hole disk-loaded structures can be readily increased by three times more than that of the conventional linear beam devices due to the more concentrated field intensity distribution in the central region.[30–32] When compared with current promising coaxial multi-beam EIKs,[28] the single tunnel size of this structure can still support an intense electron beam with a higher total current without requiring expensive and complex electron optical systems.

III. CIRCUIT CHARACTERISTICS AND STABILITY ANALYSIS

The designed overmoded structure provides a significant step toward solving the size and power constraints of the device, but multi-mode coexistence and mode competition are naturally enhanced in more oversized high-frequency structures. All of these efforts are justified because the apparent increase in the transverse dimension of the high-frequency structures relative to the wavelength allows the application of denser electron beams, which will translate into further

TABLE I. Design parameters.

Symbol	Description	Value and unit
d_{in}	Beam tunnel diameter of UGS	3.60 mm
d_{out}	Center disk outer diameter of UGS	10.54 mm
r	Coupling hole radius of UGS	2.88 mm
t	Coupling hole angular width of UGS	60°
h	Entire cavity diameter of UGS	16.30 mm
Nd_{in}	Beam tunnel diameter of NUGS	3.60 mm
Nd_{out}	Center disk outer diameter of NUGS	11.10 mm
Nc	Groove diameter of NUGS	7.00 mm
Nr	Coupling hole radius of NUGS	2.88 mm
Nt	Coupling hole angular width of NUGS	60°
Nh	Entire cavity diameter of NUGS	16.86 mm

improvements in power generation. Beam–wave interaction theory of classical linear beam devices notes that the electron beam interacts with the E_z component of the electric field in the central region.[35] Therefore, TM_{0n} modes preferably interact with the electron beam on the central axis, where the index n is determined by the variation in the distribution pattern of the axial electric field along the radial direction. Since the designed circuit is based on a finite period structure realized in a disk-loaded coupled cavity, a number of discrete frequencies are generated by the number of half-wavelengths between the cavity end walls. Typically, the greater the number of periods contained in each cavity, the more discrete modes there will be. To reduce the adverse effects caused by mode competition, we use the two-gap structure to form the front input cavity and the middle buncher cavity of the designed EIK and use the three-gap structure as the output cavity.

The operating mode field characteristics of the four-coupling-hole disk-loaded structure are studied using commercially available 3D electromagnetic finite element analysis software (CST Microwave Studio).[36,37] Figures 3(a) and 3(b) show the dispersion characteristics of the two structures, respectively. The axial mode is planned as the 2π mode that provides an electric field in the same direction on each gap, which ensures the effective modulation of the electron beam. Due to the E_z-field distribution within the beam tunnel region of the interaction gap, discrete modes of TM_{01} are considered as potentially competing risks to the desired TM_{02} mode. To weaken the E_z-field strength of the TM_{01} mode at the center of the gap, we further propose an improved non-uniform gap structure (NUGS) based on the original uniform gap structure (UGS), as shown in Fig. 2(b). Figure 4 shows the E_z-field magnitude distributions for the desired working mode and the undesired competing mode for the UGS and the NUGS. The sudden change of the electric field intensity in the beam tunnel area caused by the non-uniformity of the gap width is related to the difference of the field distribution of the TM_{01} and TM_{02} modes. Because the half-standing wave numbers of TM_{01} mode and TM_{02} mode distributed radially in the gap are different, changing the width of the gap has the effect of adjusting the energy storage and thus changing the field distribution. As shown in Fig. 4, the E_z-field strength at and near the central axis of the TM_{02} mode is further enhanced by reducing the width of the outer edge portion of the gap. At the same time, the E_z-field strength of TM_{01} mode at and near the central axis is weakened. For comparison reasons, we further normalize the E_z-field amplitude
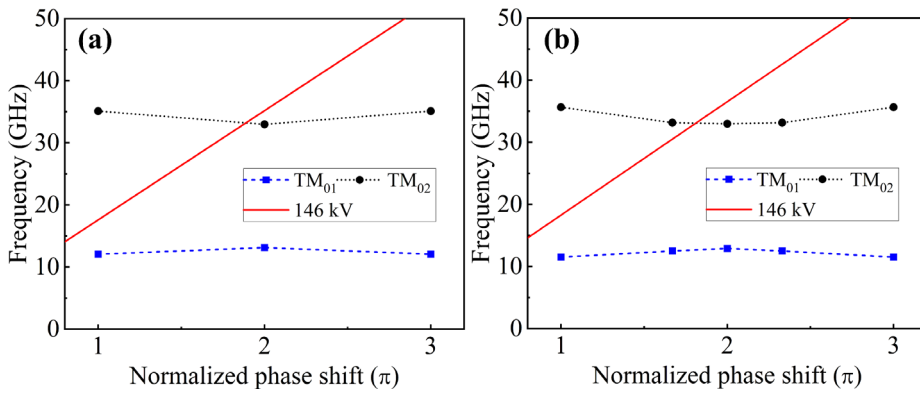
FIG. 3. Dispersion diagrams of (a) two-gap cavity and (b) three-gap cavity.

of each mode field along the axial direction in the beam tunnel, as shown in Fig. 5. We find that the TM$_{02}$ mode of the NUGS has the strongest E_z-field amplitude at the central axis compared with other modes.

The different field distributions of these two structures also affects the high-frequency characteristic parameters. Coupling coefficient M and characteristic impedance R/Q of the resonant circuit are important and commonly used indices that capture the energy coupling between the high-frequency field and electron beam. R/Q and M can be assessed from[37]

$$\frac{R}{Q} = \frac{\left(\int |E_z| \cdot dl \right)^2}{2\omega W},$$ (1)

$$M(\beta_e) = \frac{\int_{-\infty}^{\infty} E(z)e^{j\beta_e z}dz}{\int_{-\infty}^{\infty} |E(z)|dz},$$ (2)

where ω is the angular frequency, W is the total stored energy, $E(z)$ is the longitudinal field distribution, and β_e is the propagation constant of the electron beam. The effective characteristic impedance $M^2 R/Q$ is widely used to evaluate the beam–wave coupling performance.[38] The product $M^2 R/Q$ is considered to be positively correlated with the proactive interaction between the electron beam and the mode field. Our findings for the UGS and the NUGS are summarized in Fig. 6(a). Due to the enhancement of the field strength in the beam tunnel region within the gap, the NUGS greatly increases the $M^2 R/Q$ value of the TM$_{02}$ mode. Furthermore, the NUGS also reduces the $M^2 R/Q$ of the competing TM$_{01}$ mode compared to the UGS. Field analysis for both structures is verified here (as shown in Fig. 4), highlighting the functional advantage of the NUGS for suppressing low-order TM$_{01}$ mode.

In the intermediate cavity of the EIK, self-oscillation of the working mode, or oscillation of the undesired modes, will greatly perturb the electron bunching so as to distort the normal signal amplification. The total quality factor Q_t is a common technical figure of merit for evaluating the self-oscillation of interacting circuits, expressed as[39]
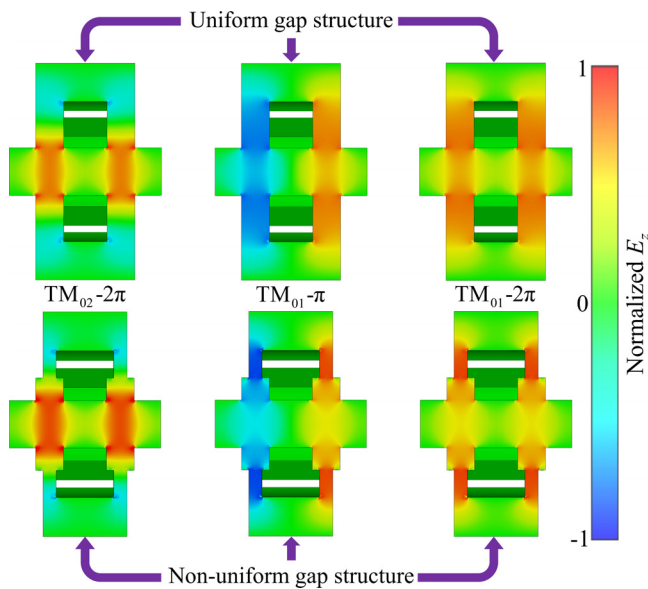

FIG. 4. The E_z-field magnitude distributions for the desired working mode and the undesired competing mode for the UGS and the NUGS.
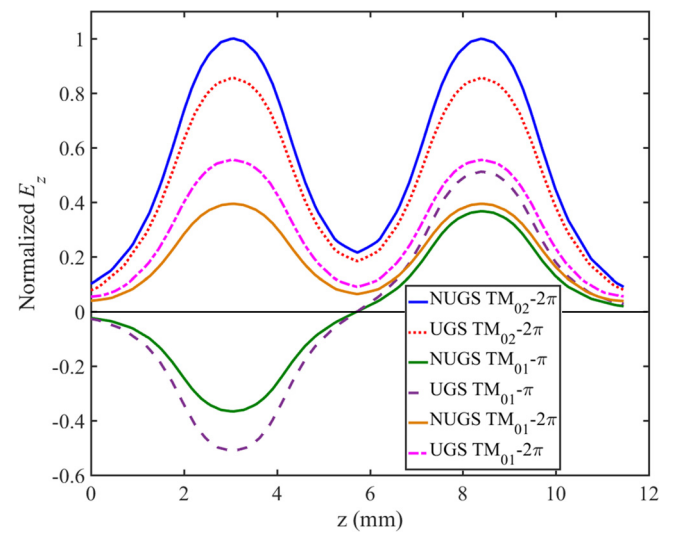

FIG. 5. Distribution of the E_z-field amplitude along the axial direction in the beam tunnel of each mode of the UGS and the NUGS.
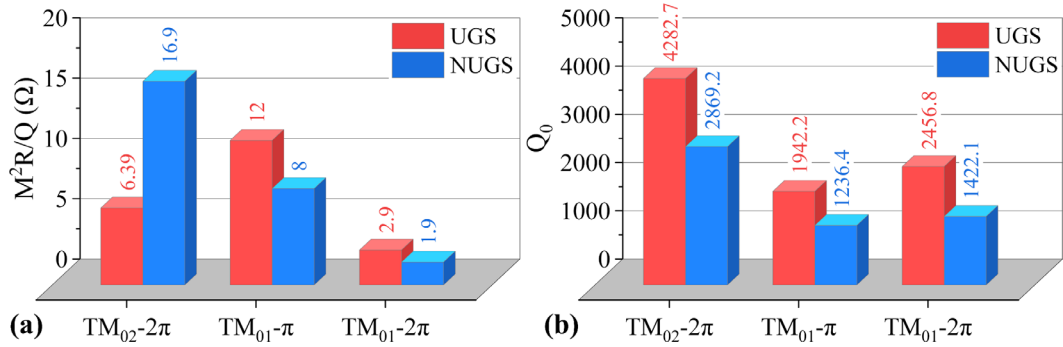
FIG. 6. (a) Effective characteristic impedance M^2R/Q and (b) intrinsic quality factor Q_0 of the UGS and the NUGS.

$$\frac{1}{Q_t} = \frac{1}{Q_0} + \frac{1}{Q_e} + \frac{1}{Q_b}, \qquad (3)$$

where Q_0 and Q_e are the intrinsic quality factor and externally loaded quality factor, respectively. Figure 6(b) shows Q_0 for both structures. Q_b is beam-loaded quality factor, defined as[24]

$$\frac{1}{Q_b} = G_e\left(\frac{R}{Q}\right), \qquad (4)$$

where G_e is the beam-load conductance. G_e is derived from the space-charge wave theory, expressed as[40,41]

$$G_e = \frac{1}{8}\frac{\beta_e}{\beta_q}G_0\left[|M_-^2(\beta_e - \beta_q)| - |M_+^2(\beta_e + \beta_q)|\right], \qquad (5)$$

where β_q is the propagation constants of the reduced plasma. G_0 is the DC conductance of the electron beam. $M_-(\beta_e - \beta_q)$ and $M_+(\beta_e + \beta_q)$ represent the coupling coefficients of fast and slow space charge waves. Here, g_e represents the ability to transfer energy from the electron beam to the circuit, where $g_e = G_e/G_0$. Negative g_e indicates that the DC energy of the electron beam is converted into high-frequency field energy, and this mode may be excited. A larger peak value of the negative g_e suggests that the mode field is more readily excited during oscillation. To maintain the stability of the oscillating circuit, it is necessary that the lossy conductive wall and the external load fully absorb the energy released by the electron beam.[42] When $Q_t < 0$, the

oscillating circuit will have a tendency to start oscillating.[39] Here, to avoid self-oscillation, $Q_t > 0$ is required. Q_e is infinite for an unloaded intermediate cavity, while Q_0 is related to the inner wall Ohmic losses and is always positive. Therefore, Q_b should also be as positive as possible. As a result, $g_e > 0$ is required in the appropriate beam voltage range. Figures 7(a) and 7(b) show the change of the g_e with the electron beam DC voltage for these two structures, respectively. Through the analysis of the beam–wave synchronization conditions, when the operating voltage is set between 100 and 150 kV, the resonant modes near the beamline will not self-oscillate.

Based on the four-coupling-hole disk-loaded structure, a Ka-band EIK consisting of an input cavity, four middle cavities, and an output cavity has been designed, as shown in Fig. 8. An important advantage of this overmoded structure, compared with the conventional ladder-type interaction circuits,[23] is that the maximum axial field energy of the TM_{02} mode can be directly coupled to the output waveguide through simple aperture diffraction. The condition for coupling between the main and secondary resonators or waveguides through the small aperture is that the normal component of the electric field or the tangential component of the magnetic field in the same direction exist in the main and secondary resonators or waveguides at the same time, and these components cannot be zero at the same time at the position of the small aperture. Since the TM_{02} mode has a normal electric field perpendicular to the common wall, through a small hole opened on the central axis of the end of the cavity, the electric field lines will pass through the small hole and excite the TM_{01} mode
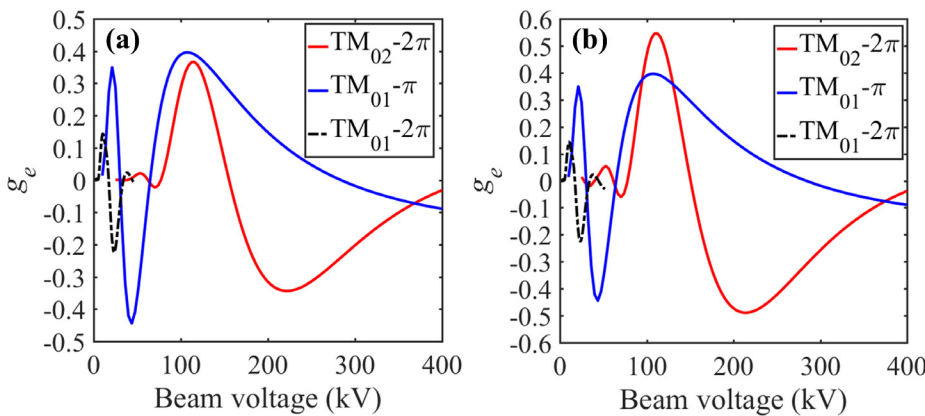

FIG. 7. The g_e of the (a) UGS and the (b) NUGS as a function of the electron beam voltage.
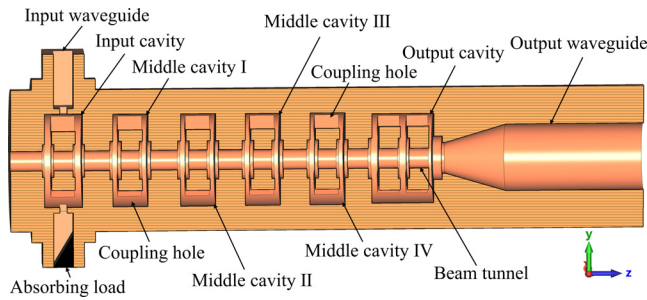
FIG. 8. Schematic diagram of a six-cavity *Ka*-band extended interaction klystron (EIK).

field in the output waveguide to propagate, as shown in Fig. 9(a). Here, we use the group delay time method to solve the diffraction quality factor of the output cavity.[42] The Q_e obtained by the group delay time is 177 at 32.94 GHz, as shown in Fig. 9(b). Table II lists the physical parameters of each cavity, where f is the resonant frequency, p is the period length.

IV. PIC SIMULATION RESULT AND ANALYSIS

To verify the stability and beam–wave interaction capability of the overmoded circuit, 3D PIC simulations have been carried out for the EIK using CST. Since the EIK only requires single-beam operation and has an oversized beam tunnel, a conventional Pierce electron gun can be used to drive this highly overmoded circuit, and a uniform permanent magnet system can be used to maintain the focus of the electron beam.[35] Assuming pulsed operation, an electron beam with a diameter of 3.3 mm and a current of 24 A is injected into the high-frequency circuit at a bias of 146 kV. A constant magnetic field of 0.55 T is used to focus the electron beam. To retain realism in the simulations, we use reduced effective conductivity values to replace the extra Ohmic losses caused by surface roughness. The conductivity of the cavity wall is set to 3.6×10^7 S/m, corresponding to a surface roughness of 0.15 μm, which is about 62% of the ideal conductivity of oxygen-free copper.[43] As shown in Fig. 8, the input cavity adopts a dual waveguide port configuration. One waveguide port is connected to the excitation signal source and the other waveguide port is connected to the absorbing load, so as to improve the working bandwidth. The specifications for both waveguides are standard WR-28 waveguides.

TABLE II. Parameters of each cavity.

Cavity	f (GHz)	p (mm)	$M^2(R/Q)$ (Ω)	Q_t
Input cavity	32.90	5.56	39.8	68
Middle cavity I	32.84	5.36	16.6	1279
Middle cavity II	32.89	5.36	16.7	1277
Middle cavity III	32.93	5.36	16.8	1274
Middle cavity IV	32.98	5.36	16.9	1271
Output cavity	32.92	5.16	16.9	177

Figure 10(a) shows the output signal, output power, and its spectrum when the input power is 2 W at 32.94 GHz. A maximum output power of 1.11 MW is obtained at 32.94 GHz in the circular waveguide TM_{01} mode, with a corresponding gain and efficiency of 57 dB and 31.7%, respectively. As shown in Fig. 10(b), the maximum field strength of the cavity is 38.12 MV/m, which is less than the vacuum breakdown field strength (145 MV/m).[44] The inset of Fig. 10(b) shows the beam modulation and bunching during interactions with the operating mode. Figure 10(c) shows the output power as a function of the input signal sweep-frequency for a representative input power of 2 W. The 3-dB bandwidth reaches 120 MHz, from 32.84 to 32.96 GHz. Figure 10(d) shows the effect of input power on output performance. When closer to the edge of the operating band, especially at the high frequency end, more input power is required to drive this EIK into saturation. Figure 11 shows the electron beam trajectory after the output signal has stabilized. During the entire beam–wave interaction, the electron beam is modulated and bunches are generated in the longitudinal direction. Figure 12 shows the output power, beam–wave interaction efficiency, and beam transparency as a function of the diameter of the electron beam. The electron beam with a diameter of 3.3 mm can stably drive the EIK to produce a large peak power and has a beam transparency higher than 99.6%. Thus, this can be considered as a design parameter for optimal beam–wave interaction. Even in engineering, the diameter of the electron beam can still be adjusted to ensure the stable operation of the device within the tolerance range.

V. CONCLUSION

The substantial increase in the output power of conventional linear beam devices has proven a significant and ongoing technical challenge throughout a wide variety of scientific, commercial, and military
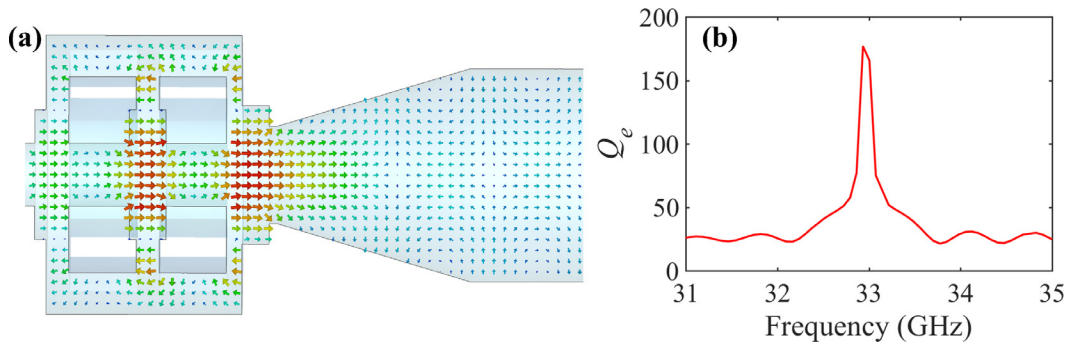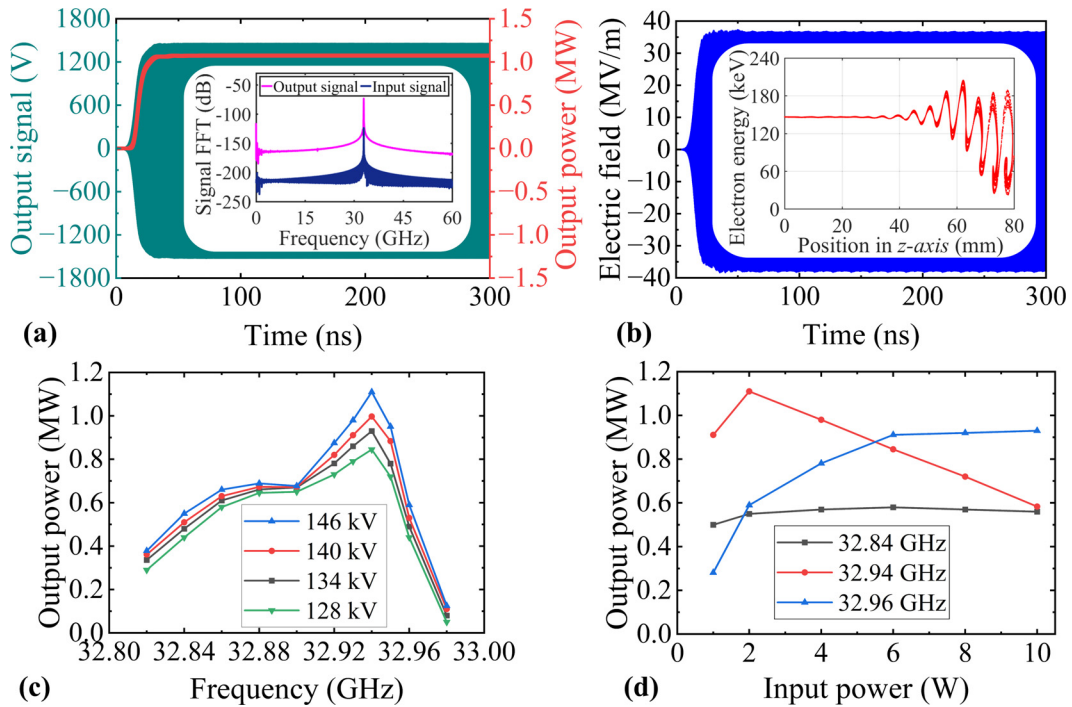

FIG. 9. (a) Simulated electric field distribution on the longitudinal section of the output cavity. (b) The Q_e of output circuit calculated by group delay.

FIG. 10. (a) Output signal power showing MW generation. Inset: frequency spectra of the input and output signals. (b) Amplitude at the gap in the output cavity where the electric field is strongest. Inset: phase-space diagram of electron energy. (c) Output power as a function of input signal sweep frequency characteristics. (d) Output power as a function of input power.
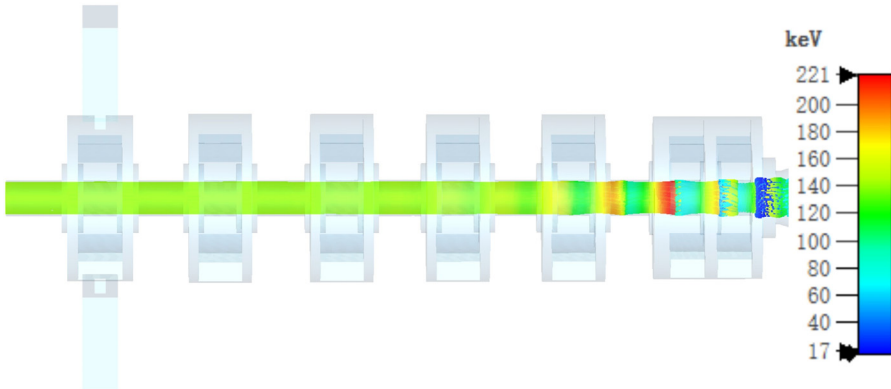
FIG. 11. 3D electron beam trajectory during the entire beam–wave interaction.
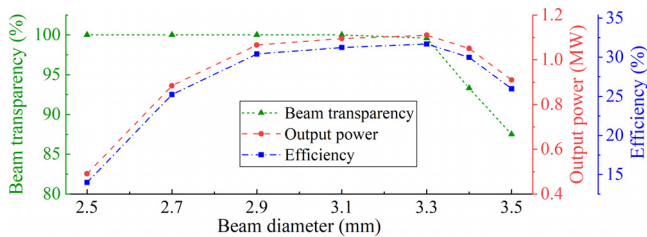
FIG. 12. Effect of electron beam diameter on output power, beam–wave interaction efficiency, and beam transparency.

activities. In order to realize the high-current electron beam loading capability of compact devices, an overmoded interaction circuit with a larger beam tunnel size than conventional structures is designed. Even compared to the promising multi-beam and sheet-beam structures, its single tunnel can still support an intense electron beam with a high total current without the need for complex electron optical system and focusing system. Through the optimized analysis of high-frequency characteristics, the four-coupling-hole disk-loaded interaction circuit operating in TM_{02} mode shows worthwhile potential in overcoming the output power limitations, improving the beam–wave coupling ability and operating stability. A MW-class *Ka*-Band EIK operating stably

in the TM_{02} mode based on this structure has been verified by 3D PIC simulation. Such new design approaches are expected to be used to develop coherent electromagnetic radiation sources with higher frequency, higher power, and higher efficiency.

AUTHOR DECLARATIONS

Conflict of Interest

The authors have no conflicts to disclose.

Author Contributions

Yifan Zu: Conceptualization (lead); Data curation (lead); Formal analysis (lead); Investigation (lead); Methodology (lead); Project administration (lead); Resources (lead); Software (lead); Validation (lead); Visualization (lead); Writing – original draft (lead); Writing – review & editing (lead). **Yang Yan:** Funding acquisition (equal); Supervision (equal). **Xuesong Yuan:** Conceptualization (lead); Data curation (equal); Formal analysis (equal); Funding acquisition (lead); Investigation (equal); Methodology (equal); Project administration (equal); Resources (equal); Writing – original draft (equal); Writing – review & editing (equal). **Xiaotao Xu:** Investigation (equal). **Qingyun Chen:** Investigation (equal). **Matthew Thomas Cole:** Conceptualization (equal); Formal analysis (equal); Supervision (equal); Writing – original draft (lead); Writing – review & editing (lead). **Yong Yin:** Conceptualization (equal); Investigation (equal); Methodology (equal); Project administration (equal). **Hailong Li:** Supervision (equal). **Bin Wang:** Supervision (equal). **Lin Meng:** Funding acquisition (equal); Supervision (equal).

DATA AVAILABILITY

The data that support the findings of this study are available from the corresponding author upon reasonable request.

REFERENCES

[1] Y. Gong, Q. Zhou, M. Hu, Y. Zhang, X. Li, H. Gong, J. Wang, D. Liu, Y. Liu, Z. Duan, and J. Feng, "Some advances in theory and experiment of high-frequency vacuum electron devices in China," IEEE Trans. Plasma Sci. **47**(5), 1971–1990 (2019).

[2] N. C. Luhmann, Jr., H. Bindslev, H. Park, J. Sanchez, G. Taylor, and C. X. Yu, "Microwave diagnostics," Fusion Sci. Technol. **53**(2), 335–396 (2008).

[3] L. Krier, I. G. Pagonakis, K. A. Avramidis, G. Gantenbein, S. Illy, J. Jelonnek, J. Jin, H. P. Laqua, A. Marek, D. Moseev, and M. Thumm, "Theoretical investigation on possible operation of a 140 GHz 1 MW gyrotron at 175 GHz for CTS plasma diagnostics at W7-X," Phys. Plasmas **27**(11), 113107 (2020).

[4] V. L. Granatstein, R. K. Parker, and C. M. Armstrong, "Vacuum electronics at the dawn of the twenty-first century," Proc. IEEE **87**(5), 702–716 (1999).

[5] J. Benford, J. A. Swegle, and E. Schamiloglu, *High Power Microwaves*, 3rd ed. (Taylor & Francis, New York, 2016).

[6] A. Mase, Y. Kogi, D. Kuwahara, Y. Nagayama, N. Ito, T. Maruyama, H. Ikezi, X. Wang, M. Inutake, T. Tokuzawa, J. Kohagura, M. Yoshikawa, S. Shinohara, A. Suzuki, F. Sakai, M. Yamashika, B. J. Tobias, C. Muscatello, X. Ren, M. Chen, C. W. Domier, and N. C. Luhmann, "Development and application of radar reflectometer using micro to infrared waves," Adv. Phys.-X **3**(1), 633–675 (2018).

[7] D. K. Abe, J. P. Calame, C. D. Joye, A. M. Cook, J. Pasour, S. Cooke, A. N. Vlasov, I. A. Chernyavskiy, B. Levush, K. T. Nguyen, D. E. Pershing, and D. Chernin, "Millimeter-wave and sub-millimeter-wave vacuum electronics amplifier development at the US Naval Research Laboratory," Proc. SPIE **8624**, 86240H (2013).

[8] L. J. R. Nix, L. Zhang, W. He, C. R. Donaldson, K. Ronald, A. W. Cross, and C. G. Whyte, "Demonstration of efficient beam-wave interaction for a MW-level 48 GHz gyroklystron amplifier," Phys. Plasmas **27**(5), 053101 (2020).

[9] R. Bingham, J. Mendonca, and P. Shukla, "Plasma based charged-particle accelerators," Plasma Phys. Controlled Fusion **46**(1), R1–R23 (2004).

[10] M. D. Abouzahra and R. K. Avent, "The 100-kW millimeter-wave radar at the Kwajalein atoll," IEEE Antennas Propag. Mag. **36**(2), 7–19 (1994).

[11] A. A. Tolkachev, B. A. Levitan, G. K. Solovjev, V. V. Veytsel, and V. E. Farber, "A megawatt power millimeter-wave phased-array radar," IEEE Aerosp. Electron. Syst. Mag. **15**(7), 25–31 (2000).

[12] T. C. Luce, "Applications of high-power millimeter waves in fusion energy research," IEEE Trans. Plasma Sci. **30**(3), 734–754 (2002).

[13] S. H. Gold and G. S. Nosinovich, "Review of high-power microwave source research," Rev. Sci. Instrum. **68**(11), 3945–3974 (1997).

[14] J. Zhang, D. Zhang, Y. Fan, J. He, X. Ge, X. Zhang, J. Ju, and T. Xun, "Progress in narrowband high-power microwave sources," Phys. Plasmas **27**(1), 010501 (2020).

[15] D. Berry, H. Deng, R. Dobbs, P. Horoyski, M. Hyttinen, A. Kingsmill, R. MacHattie, A. Roitman, E. Sokol, and B. Steer, "Practical aspects of EIK technology," IEEE Trans. Electron Devices **61**(6), 1830–1835 (2014).

[16] B. Steer, A. Roitman, P. Horoyski, M. Hyttinen, R. Dobbs, and D. Berry, "Millimeter-wave extended interaction klystrons for high power ground, airborne and space radars," in *Proceedings of 41st European Microwave Conference, Manchester* (IEEE, 2011), pp. 984–987.

[17] J. Zhao, H. Yin, L. Zhang, L. W. He, Q. Zhang, A. D. R. Phelps, and A. W. Cross, "Experiments on W-band extended interaction oscillators with pseudospark sourced post-accelerated electron beam," Phys. Plasmas **24**(6), 060703 (2017).

[18] D. H. Preist and W. J. Leidigh, "Experiments with high-power CW Klystrons using extended interaction catchers," IEEE Trans. Electron Devices **10**(3), 201–211 (1963).

[19] J. Luo, J. Feng, and Y. Gong, "A review of microwave vacuum devices in China: Theory and device development including high-power klystrons, spaceborne TWTs, and gyro-TWTs," IEEE Microwave Mag. **22**(4), 18–33 (2021).

[20] J. H. Booske, "Plasma physics and related challenges of millimeter-wave-to-terahertz and high power microwave generation," Phys. Plasmas **15**(5), 055502 (2008).

[21] J. H. Booske, R. J. Dobbs, C. D. Joye, C. L. Kory, G. R. Neil, G. S. Park, J. Park, and R. J. Temkin, "Vacuum electronic high power terahertz sources," IEEE Trans. Terahertz Sci. Technol. **1**(1), 54–75 (2011).

[22] R. K. Parker, R. H. Abrams, B. G. Danly, and B. Levush, "Vacuum electronics," IEEE Trans. Microwave Theory Tech. **50**(3), 835–845 (2002).

[23] L. Bi, L. Meng, Y. Yin, C. Xu, S. Zhu, R. Peng, F. Zeng, Z. Chang, B. Wang, H. Li, and P. Zhang, "Power enhancement for millimeter-wave extended interaction radiation sources by using the TM_{31}-mode scheme," Phys. Plasmas **26**(6), 063101 (2019).

[24] D. Wang, G. Wang, J. Wang, S. Li, P. Zeng, and Y. Teng, "A high-order mode extended interaction klystron at 0.34 THz," Phys. Plasmas **24**(2), 023106 (2017).

[25] J. Li, Z. Wu, M. Hu, R. Zhong, K. Zhang, J. Zhou, D. Liu, and S. Liu, "Research on optimized structure of a 220-GHz extended interaction oscillator," Phys. Plasmas **28**(9), 093108 (2021).

[26] J. Qing, X. Niu, T. Zhang, Y. Liu, G. Guo, and H. Li, "THz radiation from a TM_{51} mode sheet beam extended interaction oscillator with low injection," IEEE Trans. Plasma Sci. **50**(4), 1081–1086 (2022).

[27] S. Lü, C. Zhang, S. Wang, and Y. Wang, "Stability analysis of a planar multiple-beam circuit for *W*-band high-power extended-interaction klystron," IEEE Trans. Electron Devices **62**(9), 3042–3048 (2015).

27 November 2023 08:21:03

[28]X. Zhang, R. Zhang, and Y. Wang, "Study of a dual-mode multibeam interaction circuit with coaxial structure for Ka-band high-power EIK," IEEE Trans. Electron Devices **68**(2), 822–828 (2021).

[29]J. C. Cai, I. Syratchev, and G. Burt, "Design study of a high-power *Ka*-band high-order-mode multibeam klystron," IEEE Trans. Electron Devices **67**(12), 5736–5742 (2020).

[30]D. Zhao, W. Gu, X. Hou, G. Liu, Q. Xue, and Z. Zhang, "Demonstration of a high-power *Ka*-band extended interaction klystron," IEEE Trans. Electron Devices **67**(9), 3788–3794 (2020).

[31]H. Gong, Y. Gong, T. Tang, J. Xu, and W.-X. Wang, "Experimental investigation of a high-power Ka-band folded waveguide traveling-wave tube," IEEE Trans. Electron Devices **58**(7), 2159–2163 (2011).

[32]C. Paoloni, M. Mineo, M. Henry, and P. G. Huggard, "Double corrugated waveguide for Ka-band traveling wave tube," IEEE Trans. Electron Devices **62**(11), 3851–3856 (2015).

[33]Y. Zu, Y. Lan, X. Yuan, X. Xu, Q. Chen, H. Li, M. T. Cole, Y. Yin, B. Wang, L. Meng, and Y. Yan, "Research on a highly overmoded slow wave circuit for 0.3-THz extended interaction oscillator," IEEE Trans. Electron Devices **70**(4), 2165–2169 (2023).

[34]D. M. Pozar, *Microwave Engineering*, 4th ed. (Wiley, New York, 2011).

[35]A. S. Gilmour and I. Ebrary, *Klystrons, Traveling Wave Tubes, Magnetrons, Crossed-Field Amplifiers, and Gyrotrons* (Artech HouseBooks, Norwood, 2011).

[36]See www.cst.com/Products/csts2 for "CST-Computer Simulation Technology."

[37]C. Xu, B. Wang, R. Peng, L. Bi, F. Zeng, Z. Chang, S. Zhu, Y. Yin, H. Li, and L. Meng, "Start current study of a THz sheet beam extended interaction oscillator," Phys. Plasmas **25**(7), 073103 (2018).

[38]N. Guo, Z. Qu, X. Shang, H. Ding, K. Liu, W. Song, H. Wang, J. Wang, D. Zhao, and Q. Xue, "Analysis and improvement of performance instability in extended interaction klystrons with random geometrical perturbations," IEEE Trans. Electron Devices **69**(10), 5886–5894 (2022).

[39]X. Xu, X. Yuan, H. Li, Q. Chen, Y. Zu, M. Cole, J. Xie, Y. Yin, and Y. Yan, "Design of a G-band extended interaction klystron based on a three-coupling-hole structure," IEEE Trans. Electron Devices **69**(3), 1368–1373 (2022).

[40]S. Li, J. Wang, G. Wang, and D. Wang, "Theoretical studies on stability and feasibility of 0.34 THz EIK," Phys. Plasmas **24**(5), 053107 (2017).

[41]M. Chodorow and T. Wessel-Berg, "A high-efficiency klystron with distributed interaction," IRE Trans. Electron Devices **8**(1), 44–55 (1961).

[42]Y. Ding, *Theory and Computer Simulation of High Power Klystron* (National Defense Industry Press, Beijing, China, 2008), pp. 44–47.

[43]S. K. Datta, L. Kumar, and B. N. Basu, "A simple and accurate analysis of conductivity loss in millimeter-wave helical slow-wave structures," J. Infrared, Millimeter, Terahertz Waves **30**(4), 381–392 (2009).

[44]W. Peter, R. J. Faehl, A. Kadish, and L. E. Thode, "Criteria for vacuum breakdown in RF cavities," IEEE Trans. Nucl. Sci **30**(4), 3454–3456 (1983).

27 November 2023 08:21:03